RSC Advances

PAPER

View Article Online
View Journal | View Issue

Cite this: *RSC Adv.*, 2022, **12**, 15741

4,4′-Dimethoxybenzhydryl substituent augments performance of bis(imino)pyridine cobalt-based catalysts in ethylene polymerization†

Shi-Fang Yuan,*[a] Luyao Wang,[ab] Yi Yan,[ab] Tian Liu,[ab] Zygmunt Flisak,*[bc] Yanping Ma[b] and Wen-Hua Sun*[b]

A series of cobalt complexes with bis(imino)pyridine derivatives featuring unsymmetrical substitution with bulky groups has been synthesized and characterized. The molecular structures of two representatives have been determined by the single-crystal X-ray diffraction study, revealing distorted tetrahedral geometry with different degrees of steric hindrance imparted by the two inequivalent aryl groups attached to the imine nitrogen atoms. On activation with either MAO or MMAO, these complexes display high activity toward ethylene polymerization, reaching 8.71 × 10^6 g of PE (mol of Co)$^{-1}$ h^{-1} at 60 °C and produce polyethylene of high molecular weight (M_w = 5.27 × 10^5 g mol^{-1}) and low dispersity. The presence of the methoxy-substituent noticeably enhances the activity of the cobalt catalyst and increases the molecular weight of the resultant polyethylene.

Received 9th March 2022
Accepted 17th May 2022

DOI: 10.1039/d2ra01547a

rsc.li/rsc-advances

1. Introduction

Seminal reports on Ni^{2+} and Pd^{2+} complexes with α-diimines[1] as well as Fe^{2+} and Co^{2+} complexes with bis(imino)pyridines[2,3] as highly active precatalysts toward ethylene polymerization have induced considerable interest in the late-transition-metal-based precatalysts within academia and industry. Recent reviews[4–10] reflect significant progress in the development of such precatalysts as researchers are encouraged to design the novel catalytic systems instrumental in the synthesis of advanced polymeric materials. Our group has long been involved in the modification of bis(imino)pyridine-based systems.[11] The structure of the catalysts can be adjusted in a wide range,[12–23] thus affecting the properties of the polymeric products. Derivation of the original model (A, Scheme 1),[2] which involves the modification of the aniline starting material,[24–38] is an example of the catalyst fine tuning. The steric hindrance introduced to these anilines (B, Scheme 1)[25] improves the catalytic activity, while the electron-withdrawing substituents (C and D, Scheme 1)[27,28] increase the molecular weight of the resultant polyethylene. Encouraged with these observations, we carried out extensive tests in order to verify our hypothesis. As a result, new promising catalytic systems exhibiting desired thermal stability and generating potentially useful polymeric products were conceived (E, F and G, Scheme 1).[33–35] Further modifications, such as substituting one of the aryl rings with the dibenzocycloheptyl groups (H, Scheme 1)[36] improved the thermal stability of the catalyst. One of the other promising templates is the methoxy-substituted benzhydryl group,[39–41] offering the high activity, appreciable lifetime and thermal stability of the iron-based catalytic systems,[41] which lead to the industrially important polyethylene of high molecular weight and high density. However, the cobalt analogs have not been explored so far and we are convinced that they are worthy detailed investigation.

In the current work, the bis(imino)pyridines bearing methoxy-substituted benzhydryl groups (**I**, Scheme 1) were synthesized together with the corresponding cobalt complexes. Significant thermal stability of the catalytic system was observed in the ethylene polymerization study and the polymer of high molecular weight was produced. We performed the optimization of the

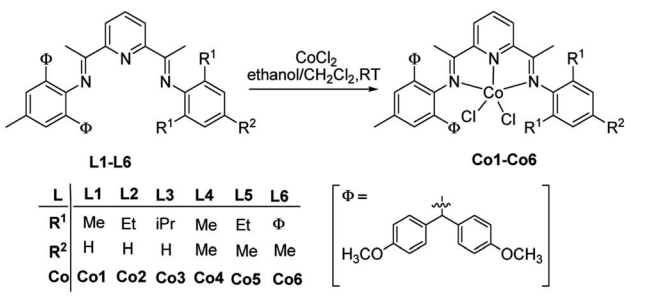

L	L1	L2	L3	L4	L5	L6
R^1	Me	Et	iPr	Me	Et	Φ
R^2	H	H	H	Me	Me	Me
Co	Co1	Co2	Co3	Co4	Co5	Co6

Scheme 1 Synthetic route to precatalysts, Co1–Co6.

[a]*The School of Chemistry and Chemical Engineering and Institute of Applied Chemistry Shanxi University, Taiyuan 030006, China. E-mail: yuansf@sxu.edu.cn*

[b]*Key Laboratory of Engineering Plastics and Beijing National Laboratory for Molecular Sciences, Institute of Chemistry Chinese Academy of Sciences, Beijing 100190, China. E-mail: whsun@iccas.ac.cn*

[c]*Faculty of Chemistry, University of Opole, Oleska 48, 45-052 Opole, Poland*

† CCDC 2124397 (**Co2**), 2124398 (**Co4**). For crystallographic data in CIF or other electronic format see **https://doi.org/10.1039/d2ra01547a**

polymerization parameters, including ethylene pressure, type and amount of the cocatalyst, reaction temperature and run time. The investigation of the properties of the resulting polyethylene, such as molecular weight, dispersity, melting point and microstructure was also carried out.

2 Experimental segment

2.1 General considerations

The air- and moisture-sensitive compounds were manipulated using Schlenk reactors under inert atmosphere of the high-purity nitrogen. Solvents were pre-treated and distilled in nitrogen before application. Most of the common solvents were exposed to sodium wire, except for dichloromethane purified by activated molecular sieves (4 Å) and ethanol dried with calcium oxide. Akzo Nobel Corp produced methylaluminoxane (MAO, toluene solution 1.46 M) and modified methylaluminoxane (MMAO, 1.93 M solution in *n*-heptane). Ethylene of polymerization quality was sourced from Yanshan, the local branch of the petrochemical company SinoPec. Other chemicals were acquired from Beijing Reagents as well as Aldrich and Acros. Nuclear magnetic resonance experiments on organometallics were conducted on a Bruker DMX 400 MHz instrument with the internal standard of tetramethylsilane (TMS) at room temperature, while the polyethylene NMR spectra were recorded using the polymer solution in deuterated 1,1,2,2-tetrachloroethane in presence of TMS at 100 °C with a Bruker DMX 300 MHz instrument. The 2000 FT IR spectrometer of PerkinElmer System was employed to record the infrared spectra and the 1112-microanalyzer of Flash EA to perform the elemental analysis. The 1,2,4-trichlorobenzene solutions of polyethylene were measured at 150 °C by a PL-GPC 220 to determine the molecular weight and dispersity; the differential scanning calorimetry traces and the melting point of polyethylene were recorded within the second scan using the DSC Q2000 instrument in the range of up to 160 °C with the heating rate of 10 °C per minute.

2.2 Preparation of [2-{{2,6-((*p*-MeOPh)$_2$CH)$_2$-4-MeC$_6$H$_2$}N=CMe}-6-{ArN=CMe)C$_5$H$_3$N]CoCl$_2$

Co1 with R1 = Me and R2 = H (Ar as 2,6-Me$_2$C$_6$H$_3$): under an inert atmosphere of nitrogen, a mixture of **L1** (0.11 g, 0.14 mmol) in dichloromethane (15 mL) and $CoCl_2$ (0.01 g, 0.14 mmol) in ethanol (5 mL) was stirred at ambient temperature for 24 h. The solution was concentrated into about 5 mL under vacuum, then 20 mL diethyl ether was added to precipitate the brown solid, which was filtrated, washed three times with 10 mL diethyl ether and finally dried to yield 0.06 g of the **Co1** brown powder (83%). ^{1}H NMR (400 MHz, $CDCl_3$, TMS): δ 112.56 (s, 1H, Py-H), 110.85 (s, 1H, Py-H), 47.06 (s, 1H, Py-H), 20.85 (s, 3H, CH_3), 9.83 (s, 2H, aryl-H$_m$), 9.27 (s, 2H, aryl-H$_m$), 6.42 (s, 4H, aryl-H), 3.31–2.73 (m, 24H, aryl-H, CH_3), 2.09 (s, 2H, 2× CH(PhOMe)$_2$), 1.18 (s, 3H, CH_3), −9.28 (s, 1H, aryl-H$_p$), −17.93 (s, 3H, CH_3), −23.94 (s, 6H, 2× N=CCH_3). FT-IR (cm^{-1}): 2979 (w), 2287 (w), 2113 (w), 1893 (w), 1737 (m), 1610 (m), 1580 (m), 1507 (s), 1459 (m), 1373 (w), 1299 (w), 1251 (s), 1174 (s), 1032 (s), 865 (s), 834 (m), 814 (w), 771 (w), 654 (m). Anal. Calcd for $C_{54}H_{53}Cl_2CoN_3O_4$ (937.87): C, 69.16; H, 5.70; N, 4.48%, found: C, 68.98; H, 5.47; N, 4.29%.

Co2 with R1 = Et and R2 = H (Ar as 2,6-Et$_2$C$_6$H$_3$): employing the similar procedure to **Co1**, 0.07 g of the **Co2** brown powder were isolated (89%). ^{1}H NMR (400 MHz, $CDCl_3$, TMS): δ 112.33 (s, 1H, Py-H), 111.05 (s, 1H, Py-H), 46.63 (s, 1H, Py-H), 21.11 (s, 3H, CH_3), 10.63 (s, 2H, aryl-H$_m$), 9.39 (s, 2H, aryl-H$_m$), 6.63 (s, 4H, aryl-H), 3.40–2.88 (m, 24H, aryl-H, CH_3), 2.19 (s, 2H, 2× CH(PhOMe)$_2$), 1.23 (s, 3H, CH_3), −9.44 (s, 1H, aryl-H$_p$), −18.12 (s, 3H, CH_3), −19.24 (s, 6H, 2× N=CCH_3), −34.93 (s, 2H, CH_2), −38.30 (s, 2H, CH_2). FT-IR (cm^{-1}): 2968 (w), 2275 (w), 2113 (w), 1894 (w), 1609 (m), 1582 (m), 1508 (s), 1459 (m), 1373 (w), 1299 (w), 1253 (s), 1177 (s), 1110 (w), 1034 (s), 870 (w), 833 (m), 811 (w), 769 (w), 658 (m). Anal. Calcd for $C_{56}H_{57}Cl_2CoN_3O_4$ (965.92): C, 69.63; H, 5.95; N, 4.35%, found: C, 69.88; H, 6.17; N, 4.16%.

Co3 with R1 = *i*Pr and R2 = H (Ar as 2,6-*i*Pr$_2$C$_6$H$_3$): similarly to **Co1**, 0.12 g of the **Co3** brown powder were collected (80%). ^{1}H NMR (400 MHz, $CDCl_3$, TMS): δ 113.57 (s, 1H, Py-H), 110.91 (s, 1H,Py-H), 48.15 (s, 1H, Py-H), 20.71 (s, 3H, CH_3), 9.90 (s, 2H, aryl-H$_m$), 9.11 (s, 2H, aryl-H$_m$), 6.60 (s, 4H, aryl-H), 3.48–2.53 (m, 24H, aryl-H, CH_3), 1.73 (s, 2H, 2× CH(PhOMe)$_2$), 1.41 (s, 2H, 2× $CHMe_2$), 1.26 (s, 3H, CH_3), −9.19 (s, 1H, aryl-H$_p$), −17.61 (s, 6H, 2× CH_3), −18.11 (s, 6H, CH_3, 2× N=CCH_3). FT-IR (cm^{-1}): 2958 (w), 2255 (w), 2113 (w), 1924 (w), 1609 (m), 1580 (m), 1507 (s), 1459 (m), 1370 (w), 1299 (w), 1247 (s), 1174 (s), 1108 (w), 1033 (s), 834 (m), 811 (w), 773 (w). Anal. Calcd for $C_{58}H_{61}Cl_2CoN_3O_4$ (993.98): C, 70.09; H, 6.19; N, 4.23%, found: C, 69.93; H, 6.02; N, 4.45%.

Co4 with R1 = R2 = Me (Ar as 2,4,6-Me$_3$C$_6$H$_2$): 0.05 g of the **Co4** brown powder were formed (79%). ^{1}H NMR (400 MHz, CD_2Cl_2, TMS): δ 112.99 (s, 1H, Py-H), 110.99 (s, 1H, Py-H), 45.35 (s, 1H, Py-H), 20.75 (s, 3H, CH_3), 20.48 (s, 3H, CH_3), 9.72 (s, 2H, aryl-H$_m$), 9.34 (s, 2H, aryl-H$_m$), 6.41 (s, 4H, aryl-H), 3.38–2.66 (m, 24H, aryl-H, CH_3), 1.97 (s, 2H, 2× CH(PhOMe)$_2$), 1.24 (s, 3H, CH_3), −18.26 (s, 3H, CH_3), −24.83 (s, 6H, 2× N=CCH_3). FT-IR (cm^{-1}): 2971 (w), 2267 (w), 2113 (w), 1913 (w), 1610 (m), 1581 (m), 1507 (s), 1457 (m), 1374 (w), 1299 (w), 1247 (s), 1174 (s), 1112 (w), 1032 (s), 834 (m), 813 (w), 736 (w). Anal. Calcd for $C_{55}H_{55}Cl_2CoN_3O_4$ (951.90): C, 69.40; H, 5.82; N, 4.41%, found: C, 69.73; H, 5.67; N, 4.23%.

Co5 with R1 = Et and R2 = Me (Ar as 2,6-Et$_2$-4-MeC$_6$H$_2$): 0.11 g of the **Co5** brown powder were obtained in (86%). ^{1}H NMR (400 MHz, $CDCl_3$, TMS): δ 111.32 (s, 1H, Py-H), 110.90 (s, 1H, Py-H), 46.69 (s, 1H, Py-H), 20.93 (s, 3H, CH_3), 20.64 (s, 3H, CH_3), 10.41 (s, 2H, aryl-H$_m$), 9.35 (s, 2H, aryl-H$_m$), 6.54 (s, 4H, aryl-H), 3.81–2.55 (m, 24H, aryl-H, CH_3), 1.81 (s, 2H, 2× CH(PhOMe)$_2$), 1.17 (s, 3H, CH_3), −17.83 (s, 3H, CH_3), −19.53 (s, 6H, 2× N=CCH_3), −34.53 (s, 2H, CH_2), −35.99 (s, 2H, CH_2). FT-IR (cm^{-1}): 2971 (w), 2259 (w), 2113 (w), 1919 (w), 1610 (m), 1581 (m), 1507 (s), 1459 (m), 1374 (w), 1299 (w), 1250 (s), 1172 (s), 1114 (w), 1032 (s), 862 (m), 834 (m), 813 (w). Anal. Calcd for $C_{57}H_{59}Cl_2CoN_3O_4$ (979.95): C, 69.86; H, 6.07; N, 4.29%, found: C, 70.09; H, 5.95; N, 4.17%.

Co6 with R1 = ϕ and R2 = Me (Ar as 2,6-ϕ_2-4-MeC$_6$H$_2$): 0.08 g of the **Co6** brown powder were obtained (81%). ^{1}H NMR (400 MHz, $CDCl_3$, TMS): δ 114.07 (s, 2H, Py-H), 111.28 (s, 1H, Py-H), 21.05 (s, 6H, CH_3), 9.21–9.16 (m, 16H, aryl-H), 8.56 (d, J =

Table 1 Crystal data and structure refinements for Co2 and Co5

	Co2	Co5
CCDC no.	2124397	2124398
Empirical formula	$C_{113}H_{115}Cl_6Co_2N_6O_8$	$C_{57}H_{59}Cl_2CoN_3O_5$
Formula weight	2015.66	995.90
Temperature, K	173.01(3)	173.00(3)
Crystal system	Monoclinic	Monoclinic
Space group	$P2_1/c$	$P2_1/n$
a, Å	12.4375(2)	9.5954(3)
b, Å	21.6032(3)	35.3574(12)
c, Å	40.2761(6)	16.2139(5)
β, °	97.5830(10)	100.772(3)
Volume, Å^3	10 727.1(3)	5403.9(3)
Z	4	4
ρ_{calc}, g cm^{-3}	1.248	1.224
μ, mm^{-1}	0.516	0.465
F (000)	4220.0	2092.0
Crystal size, mm^3	0.288 × 0.232 × 0.101	0.421 × 0.111 × 0.075
Radiation	MoKα (λ = 0.71073)	MoKα (λ = 0.71073)
2Θ range for data collection, °	6.82 to 54.998	6.886–55
Index ranges	−16 ≤ h ≤ 14, −28 ≤ k ≤ 23, −49 ≤ l ≤ 52	−11 ≤ h ≤ 12, −45 ≤ k ≤ 45, −21 ≤ l ≤ 19
Reflections collected	100 625	50 485
R (int)	0.0198	0.0602
Data/restraints/parameters	24 586/0/1234	12 395/0/614
Goodness-of-fit on F^2	1.022	1.060
Final R indexes [$I \geq 2\sigma$ (I)]	$R_1 = 0.0375$ $wR_2 = 0.0914$	$R_1 = 0.0445$ $wR_2 = 0.1129$
Final R indexes [all data]	$R_1 = 0.0427$ $wR_2 = 0.0940$	$R_1 = 0.0642$ $wR_2 = 0.1214$
Largest diff. peak/hole, (e Å^{-3})	0.98/−1.00	0.69/−0.59

8.4 Hz, 8H, aryl-H), 7.42 (d, J = 9.2 Hz, 12H, aryl-H), 3.84–2.63 (m, 48H, aryl-H, CH_3), 1.92 (s, 4H, 4× $CH(PhOMe)_2$), −19.09 (s, 6H, CH_3, 2× N=CCH_3). FT-IR (cm^{-1}): 2965 (w), 2834 (w), 1609 ($\nu_{C=N}$, m), 1581 ($\nu_{C=N}$, m), 1509 (s), 1459 (m), 1374 (w), 1298 (m), 1249 (s), 1177 (m), 1110 (m), 1032 (m), 830 (m), 776 (m), 734 (m), 688 (w). Anal. Calcd for $C_{83}H_{79}Cl_2CoN_3O_8$ (1376.39): C, 72.43; H, 5.79; N, 3.05%, found: C, 72.75; H, 5.46; N, 2.96%.

2.3 X-ray single-crystal analysis

Crystal structures of **Co2** and **Co5** were determined by the X-ray diffraction analysis. The crystals were acquired by dispersing a small amount of diethyl ether onto the dichloromethane solution of the corresponding complex at ambient temperature. The single-crystal diffraction study was performed using a XtaLAB AFC10 (RCD3) fixed-chi single diffractometer with Mo-Kα radiation (λ = 0.71073 Å) monochromated with graphite at −100(2) °C. The positions of all collected reflections were globally refined to determine the cell parameters. The intensities were corrected for empirical absorption as well as Lorentz polarization effects.[43] The nonhydrogen atoms were computed by direct methods and adjusted by full-matrix least squares on F^2 using the SHELXL-97 package, along with the hydrogen atoms localized by calculations.[42] The data related to determinations and refinements of molecular structures are collected in Table 1.

3 Result and discussion

3.1 Synthesis and characterization

The ligands (**L1–L6**) were obtained according to the literature procedure[41] from the unsymmetrically substituted anilines containing the 4,4′-dimethoxybenzhydryl group, prepared *via* Friedel–Crafts alkylation of *p*-toluidine catalyzed by zinc chloride.[44] The yellow solids **L1–L5** were purified by the column chromatography with silica gel using the eluent of ethyl acetate and petroleum ether (1 : 33). Meanwhile, the symmetrical bis(imino)pyridine **L6** (Ar = 2,6-((*p*-MeOPh)$_2$CH)$_2$-4-MeC_6H_2) was synthesized by the acid-catalyzed reaction in one step as a light-green powder and purified by the column chromatography of basic-alumina using the eluent of ethyl acetate and petroleum ether (1 : 100). The ligands reacted at room temperature for 24 hours with the molar equivalent of cobalt(II) chloride dissolved in the dichloromethane/ethanol mixture to produce the corresponding cobalt complexes (**Co1–Co6**,

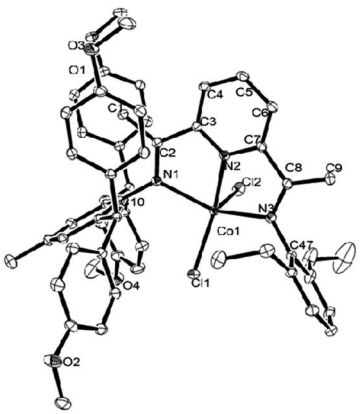

Fig. 1 ORTEP drawing of Co2 with the thermal ellipsoids set at the 30% probability level and the omission of hydrogen atoms.

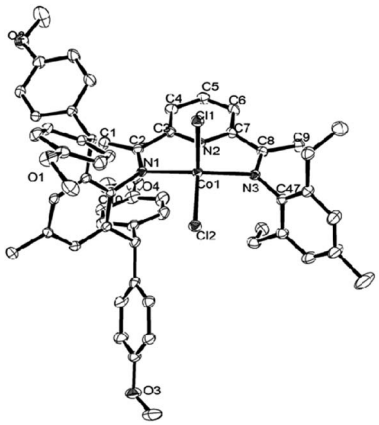

Fig. 2 ORTEP drawing of **Co5** with the thermal ellipsoids set at the 30% probability level and the omission of hydrogen atoms.

Scheme 1) with the yields between 79 and 89%. Subsequently, they were analyzed with ^{1}H NMR and FT-IR spectroscopy and the carbon, hydrogen and nitrogen content was determined. Additionally, the molecular structure of **Co2** and **Co5** species has been confirmed by the single-crystal X-ray diffraction study.

The structures are illustrated individually in Fig. 1 and 2; Table 2 shows the selected interatomic distances and angles. The two structures are similar despite the difference in the substitution pattern within the ligands (*viz.* Ar = 2,6-$Et_2C_6H_3$ in **Co2** and Ar = 2,6-Et_2-4-MeC_6H_2 in **Co5**). The coordination around the cobalt core consists of two chlorine atoms and three sp^2-hybridized nitrogen atoms of the bis(arylimino)pyridine; in this way a distorted-square pyramid with the apex of Cl and the square base of N1, N2, N3 and another Cl around cobalt ion is formed. Such five-coordinate geometry is documented for many complexes of bis(imino)pyridine cobalt(II) halides.[25,30,33,37,45] The

Table 2 Selected interatomic distances (Å) and angles (°) for **Co2** and **Co5**

	Co2	Co5
Interatomic distances		
Co(1)–N(1)	2.1740(13)	2.2184(15)
Co(1)–N(2)	2.0466(13)	2.0473(15)
Co(1)–N(3)	2.2212(13)	2.2074(16)
Co(1)–Cl(1)	2.2432(4)	2.2887(6)
Co(1)–Cl(2)	2.2921(4)	2.2512(5)
N(1)–C(2)	1.284(19)	1.290(2)
N(2)–C(7)	1.332(2)	1.334(2)
N(3)–C(8)	1.286(2)	1.285(2)
Angles		
N(1)–Co(1)–N(2)	74.51(5)	74.36(6)
N(1)–Co(1)–N(3)	141.01(5)	140.92(6)
N(2)–Co(1)–N(3)	73.87(5)	73.88(6)
N(1)–Co(1)–Cl(2)	99.99(3)	98.67(4)
N(2)–Co(1)–Cl(2)	90.81(4)	152.57(5)
N(3)–Co(1)–Cl(2)	102.67(3)	99.08(4)
N(1)–Co(1)–Cl(1)	99.76(4)	102.04(4)
N(2)–Co(1)–Cl(1)	156.46(4)	94.25(5)
N(3)–Co(1)–Cl(1)	100.15(4)	102.45(4)
Cl(1)–Co(1)–Cl(2)	112.72(19)	113.18(2)

cobalt atom sits 2.734 Å above the basal plane in **Co2** and 2.791 Å in **Co5**. Certain variations in the cobalt–nitrogen bond lengths are evident with the Co(1)–$N(2)_{pyridine}$ equal 2.0466(13) Å in **Co2**, and 2.0473(15) Å in **Co5**, respectively. These interatomic distances are markedly shorter comparing with the corresponding Co(1)–N_{imine} bonds, whose lengths are equal 2.1740(13) and 2.2212(13) Å in **Co2**; 2.2184(15) and 2.2074(16) Å in **Co5**, respectively. The change is likely caused by stronger binding to the $N_{pyridine}$ atom and the constriction of a tridentate ligand. Notwithstanding the differences in the steric properties of the inequivalent aryl groups, only modest dissimilarities in the Co–N_{imine} distances are apparent. The *N*-aryl groups are approximately perpendicular to the *N*,*N*,*N*-cobalt coordination plane with the dihedral angles of 75.04° and 83.30° in **Co2**; 73.36° and 74.40° in **Co5**, respectively. Therefore the steric properties of the *ortho*-substituents play the important role in protecting the active species.

The ^{1}H NMR spectra of **Co1–Co6** display highly shifted peaks due to the paramagnetism of the complexes. Nonetheless, some degree of assignment was possible by consideration of the proximity of the proton environments to the Co(II) ion and the comparison with the data published elsewhere.[25,27,28] By taking **Co2** (Fig. 3) as an example, the peaks for the inequivalent *meta*-pyridyl protons (F, F′) can be seen at 112.33_{av} ppm and 111.05_{av} ppm, respectively. This reflects the unsymmetrical nature of the bis(imino)pyridine ligand. Moreover, the upfield signal of *para*-pyridyl proton (**G**) appears at 46.63_{av} ppm. The *para*-methyl signal (*E*) in **Co5**, absent in **Co2**, is visible at 20.64 ppm (Fig. 4).

The FT-IR spectra of **Co1–Co6** reveal the C=N_{imine} stretching vibrations in the range of 1580–1610 cm^{-1}. These values are lower about 30 cm^{-1} in comparison with the free ligands (**L1–L6**). Such shifts in wavenumber confirm the effective coordination of the imine groups to cobalt.[25,27,33] In addition, microanalytical data were measured for both ligands and complexes.

3.2 Typical procedure for ethylene polymerization

3.2.1 Ethylene polymerization under ambient C_2H_4 pressure. In a 100 mL Schlenk reactor connected with the ethylene balloon, 30 mL toluene and 2.0 μmol **Co4** were mixed at 60 °C and then the required amount of cocatalyst (MAO or MMAO) was added by syringe. The solution was stirred for 30 min before

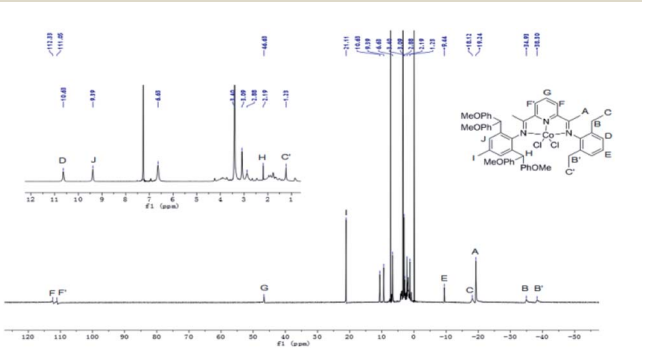

Fig. 3 ^{1}H NMR spectrum of **Co2** with an expansion of the 2–10 ppm region; recorded in $CDCl_3$ at ambient temperature.

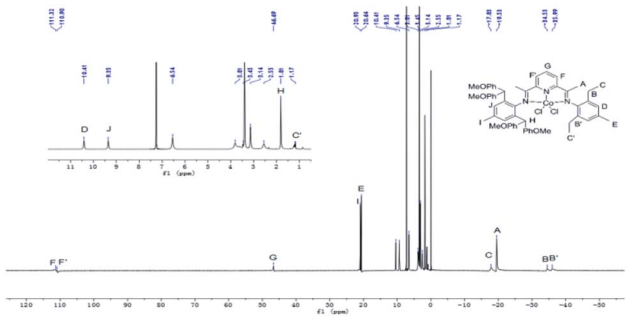

Fig. 4 ^{1}H NMR spectrum of **Co5** with an expansion of the 2–10 ppm region; recorded in $CDCl_3$ at ambient temperature.

the ethylene balloon was disconnected and the reaction was quenched by adding 5 mL 10% hydrochloric acid in ethanol. The resulting float was filtered and washed with 10 mL ethanol three times, and then dried under vacuum at 60 °C for four hours.

3.2.2 Pressurized ethylene polymerization. In a typical procedure of pressurized ethylene polymerization, a 250 mL stainless-steel autoclave fitted with pressure and temperature controllers as well as mechanical stirrer is used. Being evacuated and back-filled with high-purity nitrogen three times and finally with ethylene once, the autoclave is charged with 25 mL fresh toluene at the required temperature. Then 2.0 μmol of complex dissolved in 25 mL toluene is injected and the desired amount of cocatalyst (MAO or MMAO) as well as additional amount of toluene up to the total volume of 100 mL is added. The autoclave is immediately pressurized to the predetermined value and stirred at 400 rpm. When the polymerization test is complete, the reactor is cooled with a water bath and ethylene is vented out of the autoclave. The 10 mL 10% hydrochloric acid in ethanol is added into the reaction mixture, the polymeric float is filtered and washed with 30 mL ethanol three times. The resultant polyethylene is dried under vacuum at 60 °C for six hours.

3.2.3 Design of the experiment. In order to test the catalytic performance of the **Co1–Co6** metal complexes in the polymerization of ethylene, we conducted parallel studies on two cocatalysts, namely methylaluminoxane (MAO) and modified methylaluminoxane (MMAO), to determine how the nature of these constituents affects the performance of the catalyst. In order to gain an in-depth understanding of the catalytic properties, the effects of different reaction parameters such as ethylene feed pressure, reaction temperature, Al/Co ratio and run time were studied. To understand the physico-chemical properties of the obtained polyethylene, the gel permeation chromatography (GPC) was used to determine the molecular weight (M_w) and dispersity (M_w/M_n). The differential scanning calorimetry (DSC) was also applied to measure the melting point (T_m). In addition, ^{1}H and ^{13}C NMR spectroscopy was used to study the structural properties of the polyethylene samples.

*3.2.3.1 Optimization of reaction conditions with **Co1–Co6**/MAO.* The polymerization parameters, such as the Al/Co molar ratio, reaction temperature and time were first optimized for the **Co4** precatalyst. The results of polymerization tests with MAO at constant ethylene pressure are given in Table 3.

The Al/Co molar ratio was systematically varied with the temperature and pressure kept constant at 30 °C and 10 atm, respectively. The catalytic activity gradually increased as the

Table 3 Ethylene polymerization by using **Co1–Co6**/MAO[a]

Entry	Precatalyst	Al/Co	T, °C	t, min	Yield, g	Activity[b]	M_w[c]	M_w/M[c]	T_m[d], °C
1	**Co4**	1750	30	30	1.01	1.01	1.87	1.9	136.3
2	**Co4**	2000	30	30	1.78	1.78	3.39	1.7	136.0
3	**Co4**	2250	30	30	6.46	6.46	1.84	2.3	135.7
4	**Co4**	2500	30	30	6.75	6.75	4.37	1.9	135.5
5	**Co4**	2750	30	30	6.38	6.38	3.16	2.2	135.8
6	**Co4**	3000	30	30	4.19	4.19	3.36	2.7	135.5
7	**Co4**	2500	40	30	7.27	7.27	2.24	2.9	135.3
8	**Co4**	2500	50	30	8.63	8.63	2.25	3.1	134.8
9	**Co4**	2500	60	30	8.71	8.71	2.12	3.3	135.5
10	**Co4**	2500	70	30	3.33	3.33	0.64	1.7	135.1
11	**Co4**	2500	60	5	3.67	22.02	1.66	3.4	135.4
12	**Co4**	2500	60	15	6.03	12.06	2.01	2.9	135.0
13	**Co4**	2500	60	45	8.78	5.85	4.08	11.3	134.9
14	**Co4**	2500	60	60	9.06	4.53	5.27	8.4	135.2
15[e]	**Co4**	2500	60	30	2.71	2.71	1.39	2.8	135.5
16[f]	**Co4**	2500	60	30	1.03	1.03	0.59	2.5	133.8
17	**Co1**	2500	60	30	7.13	7.13	0.44	1.7	135.6
18	**Co2**	2500	60	30	6.37	6.37	3.38	4.7	135.4
19	**Co3**	2500	60	30	4.61	4.61	3.08	1.7	135.4
20	**Co5**	2500	60	30	7.48	7.48	2.98	3.5	135.4
21	**Co6**	2500	60	30	2.01	2.01	4.36	2.5	135.8

[a] Conditions: 2.0 μmol of **Co4**; 100 mL toluene, 10 atm ethylene (except for items 15 and 16). [b] 10^6 g (PE) mol^{-1} (Co) h^{-1}. [c] Determined by GPC; M_w: 10^5 g mol^{-1}. [d] Determined by DSC. [e] 5 atm of ethylene. [f] 1 atm of ethylene.

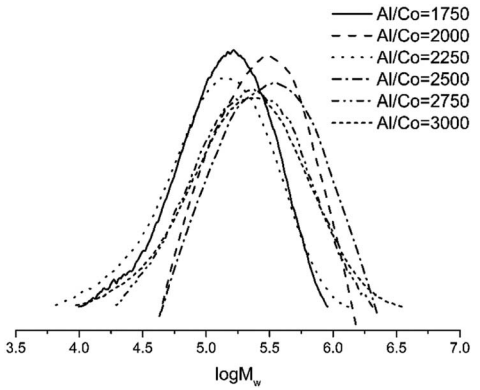

Fig. 5 GPC curves of polyethylene (entries 1–6, Table 3).

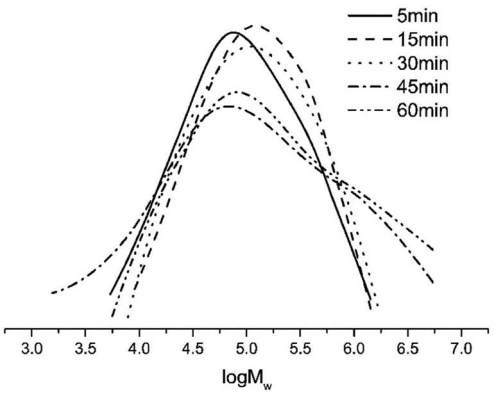

Fig. 7 GPC curves of polyethylene (entries 9 and 11–14, Table 3).

molar ratio of Al/Co was raised from 1750 to 3000 (entries 1–6, Table 3). The optimal activity of 6.75×10^6 g of PE (mol of Co)$^{-1}$ h^{-1} is observed at the Al/Co molar ratio of 2500 (entry 4, Table 3). The molecular weight of polyethylene, contained in the 1.87–4.37×10^5 g mol^{-1} range, decreases as the Al/Co molar ratio increases (Fig. 5). This is due to higher rate of chain transfer from cobalt to aluminium for the large concentrations of alkyl aluminium reagent.[20,21] The molecular weight distribution of the obtained polyethylene is relatively narrow, in the range of 1.7–2.7. Previously, similar values have also been reported.[18,46–53]

With the Al/Co molar ratio of 2500, the temperature was varied between 30 and 70 °C (entries 4 and 7–10, Table 3). The maximum catalytic activity of 8.71×10^6 g of PE (mol of Co)$^{-1}$ h^{-1} was attained at 60 °C (entry 9, Table 3). Beyond 60 °C, the activity slightly decreased due to the partial deactivation of the active species at higher temperature.[31,35,54] Nevertheless, even at 70 °C the **Co4**/MAO system maintained a remarkable value of 3.33×10^6 g of PE (mol of Co)$^{-1}$ h^{-1} (entry 10, Table 3). It was also found that the polyethylene molecular weight decreases from 4.37 to 0.64×10^5 g mol^{-1} with the temperature, which indicates higher possibility of the chain transfer and reaction termination (entries 4 and 7–10, Table 3). This trend is revealed in Fig. 6.

With the Al/Co molar ratio and the temperature of 60 °C, the ethylene polymerization by **Co4**/MAO was conducted over different reaction times from 5 to 60 min (entries 9 and 11–14, Table 3). For the reaction time of 5 min (entry 11, Table 3), the observed activity of 22.0×10^6 g of PE (mol of Co)$^{-1}$ h^{-1} was the highest value, likely indicating the rapid formation of the active species without the prolonged induction. Although the activity exhibits gradual decline with time, **Co4**/MAO still maintains the favourable value of 4.53×10^6 g of PE (mol of Co)$^{-1}$ h^{-1} for 60 min, which suggests that there is still sufficient amount of active species. It was found that the molecular weight of polyethylene shows an increasing trend with the reaction time, which is depicted in Fig. 7.

Regarding ethylene pressure, both the activity of **Co4**/MAO as well as the microstructure of the polymers obtained are greatly affected by its variations. In the experiment, the three different values of pressure, *i.e.*, 1, 5 and 10 atm were selected and the polymerization was conducted at Al/Co = 2500 and $T = 60$ °C (entries 16, 15 and 9 in Table 3). Without surprise, higher ethylene pressure results in the polyethylene of higher molecular weight. Moreover, the higher activity is also achieved, which is attributed to the increased monomer concentration.[35,55]

With the optimal conditions established for **Co4**/MAO (the Al/Co molar ratio of 2500, 60 °C and 10 atm), **Co1–Co3**, **Co5** and **Co6** were further investigated (entries 17–21, Table 3). The precatalysts displayed excellent activities ranging from 2.01 to 8.71×10^6 g of PE (mol of Co)$^{-1}$ h^{-1}. When these results are put together with those for **Co4**, the activities decrease in the following order: **Co4** [2,4,6-tri(Me)] > **Co5** [2,6-di(Et)-4-Me] > **Co1** [2,6-di(Me)] > **Co2** [2,6-di(Et)] > **Co3** [2,6-di(*i*-Pr)] > **Co6** [2,6-((*p*-MeOPh)$_2$CH)$_2$-4-MeC$_6$H$_3$]. As shown in Fig. 8, the catalytic activity of **Co4** with a methyl group at the *para* position of the phenyl ring attached to the imine nitrogen atom is higher than that of **Co1** with a hydrogen atom at the para position, indicating that the methyl electron-donating group has a positive influence on the catalytic activity. Since **Co6** has the largest steric hindrance, it also displays the lowest activity. Regarding the molecular weight of the polymer, it ranges from 0.44 to 4.36 $\times 10^5$ g mol^{-1}, with **Co6** [2,6-((*p*-MeOPh)$_2$CH)$_2$-4-MeC$_6$H$_3$] showing the highest value (entry 21, Table 3). This indicates that the large steric hindrance in the **Co6**/MAO system suppresses

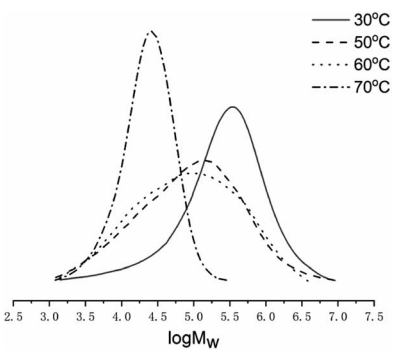

Fig. 6 GPC curves of polyethylene (entries 4 and 7–10, Table 3).

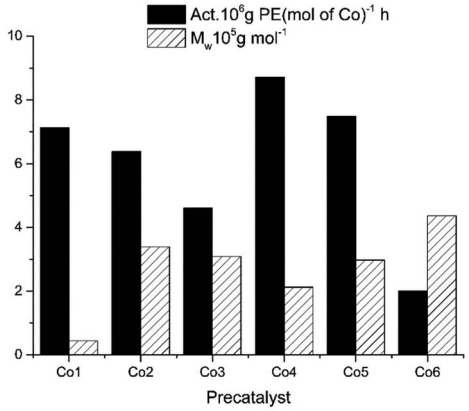

Fig. 8 Activity of the **Co1–Co6**/MAO systems and the polyethylene molecular weight.

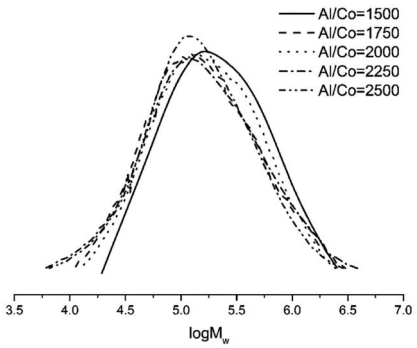

Fig. 9 GPC curves of polyethylene (entries 1–5, Table 4).

the termination reactions, which results in polyethylene of relatively high molecular weight.

*3.2.3.2 Optimization of reaction conditions with **Co1–Co6**/MMAO.* With the ethylene pressure established at 10 atm in most of the cases, the other conditions of polymerization were again optimized for **Co4**/MMAO. These are the Al/Co molar ratio, reaction temperature and reaction time. The results of polymerization tests are collected in Table 4. It was found that under comparable conditions, the **Co4**/MAO system typically displays higher activity in ethylene polymerization compared with **Co4**/MMAO.

First, the aluminium to cobalt molar ratio was varied from 1500 to 2500 and the reaction was carried out at 30 °C (entries 1–5, Table 4). The highest activity for **Co4/MMAO**, equal 5.43×10^6 g of PE (mol of Co)$^{-1}$ h^{-1}, was achieved at Al/Co = 2000 and the polymer of high molecular weight reaching 2.79×10^5 g mol^{-1} was produced. Polyethylene obtained with different values of Al/Co molar ratio showed slight variation in dispersity and no clear trend regarding the effect of the amount of cocatalyst on the molecular weight of the polyethylene could be determined, as illustrated in Fig. 9.

With the Al/Co molar ratio set at 2000, the polymerization temperature was varied between 20 and 70 °C (entries 3 and 6–10, Table 4). The activity of 5.43×10^6 g of PE (mol of Co)$^{-1}$ h^{-1} (entry 3, Table 4) was achieved at 30 °C. With elevating the reaction temperature, the activity gradually decreased to a minimum at 70 °C (entry 10, Table 4). Clearly, at higher temperature the polyethylene of lower molecular weight is generated due to increase in termination reaction rates. As an

Table 4 Ethylene polymerization using **Co1–Co6**/MMAO[a]

Entry	Precatalyst	Al/Co	T, °C	t, min	Yield, g	Activity[b]	M_w[c]	M_w/M_n[c]	T_m[d], °C
1	**Co4**	1500	30	30	4.24	4.24	3.27	2.5	135.6
2	**Co4**	1750	30	30	4.96	4.96	2.73	3.0	135.6
3	**Co4**	2000	30	30	5.43	5.43	2.79	2.7	135.6
4	**Co4**	2250	30	30	4.35	4.35	2.86	3.4	135.6
5	**Co4**	2500	30	30	3.82	3.82	2.43	2.8	135.2
6	**Co4**	2000	20	30	4.23	4.23	2.55	2.9	135.0
7	**Co4**	2000	40	30	4.52	4.52	1.61	3.3	134.6
8	**Co4**	2000	50	30	4.01	4.01	1.01	2.4	134.8
9	**Co4**	2000	60	30	3.92	3.92	0.55	2.3	134.9
10	**Co4**	2000	70	30	3.23	3.23	0.47	2.0	134.7
11	**Co4**	2000	30	5	3.19	19.14	1.57	2.0	135.3
12	**Co4**	2000	30	15	3.96	7.43	1.70	2.1	135.8
13	**Co4**	2000	30	45	7.04	4.69	3.25	4.6	136.2
14	**Co4**	2000	30	60	8.03	4.02	3.95	3.8	136.3
15[e]	**Co4**	2000	30	30	2.78	2.78	1.89	1.8	135.9
16[f]	**Co4**	2000	30	30	1.28	1.28	1.44	2.4	134.8
17	**Co1**	2000	30	30	4.31	4.31	0.64	3.0	134.9
18	**Co2**	2000	30	30	3.88	3.88	3.30	2.6	135.3
19	**Co3**	2000	30	30	4.61	4.61	3.67	3.8	135.5
20	**Co5**	2000	30	30	3.36	3.36	3.89	2.1	135.7
21	**Co6**	2000	30	30	1.12	1.12	4.49	3.6	135.8

[a] Conditions: 2.0 μmol of **Co4**; 100 mL toluene, 10 atm ethylene (except for items 15 and 16). [b] 10^6 g (PE) mol^{-1} (Co) h^{-1}. [c] Determined by GPC; M_w: 10^5 g mol^{-1}. [d] Determined by DSC. [e] 5 atm of ethylene. [f] 1 atm of ethylene.

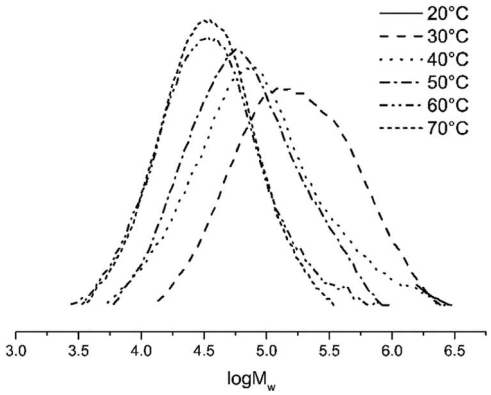

Fig. 10 GPC curves of polyethylene (entries 3 and 6–10, Table 4).

example, the molecular weight of the polymer obtained at 30 °C is equal 2.79 × 10^5 g mol^{-1}, while the polymer of molecular weight equal 0.47 × 10^5 g mol^{-1} is formed at 70 °C (entries 3 and 10, Table 4); see also Fig. 10.

To evaluate the influence of the reaction time on the performance of the **Co4**/MMAO system, ethylene polymerization was conducted for 5, 15, 30, 45, and 60 min at 30 °C and the Al/Co molar ratio of 2000 (entries 3 and 11–14, Table 4). The maximum activity reaching 19.14 × 10^6 g of PE (mol of Co)$^{-1}$ h^{-1} was observed at 5 min. Beyond this point, the activity continuously drops to reach the minimum of 4.02 × 10^6 g of PE (mol of Co)$^{-1}$ h^{-1} at 60 min due to slow deactivation of the active species. Conversely, the polyethylene molecular weight slowly increases over time (Fig. 11).

Polymerization tests performed under 5 and 1 atm of ethylene (entries 15 and 16, Table 4) indicate that low ethylene pressure leads to decline in the activity. Therefore the optimum reaction conditions for **Co4**/MMAO were established at the Al/Co molar ratio of 2000, temperature of 30 °C and ethylene pressure of 10 atm. Under the above optimal conditions, the study of the MMAO catalytic system was conducted for the **Co1–Co3**, **Co5** and **Co6** (entries 17–21, Table 4) and high activities ranging from 1.12 to 5.43 × 10^6 g of PE (mol of Co)$^{-1}$ h^{-1} were found. The order of activity for the MMAO as a cocatalyst is now

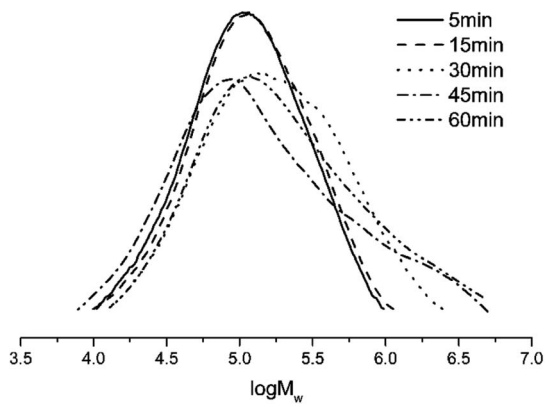

Fig. 11 GPC curves of polyethylene (entries 3 and 11–14, Table 4).

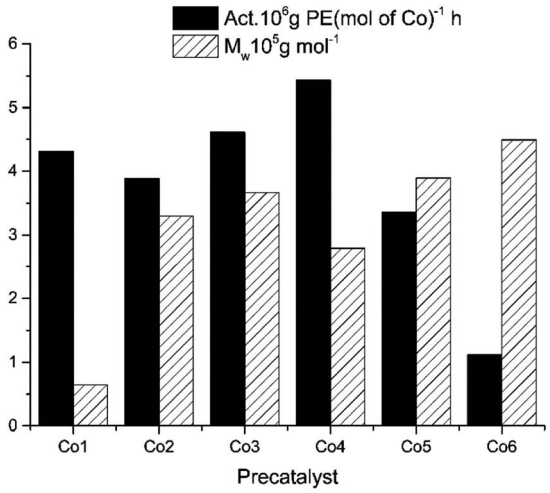

Fig. 12 Activity of the **Co1–Co6**/MMAO systems and the polyethylene molecular weight.

as follows: **Co4** [2,4,6-tri(Me)] > **Co3** [2,6-di(*i*-Pr)] > **Co1** [2,6-di(Me)] > **Co2** [2,6-di(Et)] > **Co5** [2,6-di(Et)-4-Me] > **Co6** [2,6-((*p*-MeOPh)$_2$CH)$_2$-4-MeC$_6$H$_3$] – see Fig. 12. Like in the case of MAO, **Co4** exhibits the highest activity and the molecular weight of the polymer ranges from 0.64 to 4.49 × 10^5 g mol^{-1}. The **Co6** complex produces polyethylene of the highest molecular weight, which is equal 6.29 × 10^5 g mol^{-1}. This fact indicates that the steric hindrance in **Co6** also decreases the termination rate.[20,33]

To enable comparison with the previously synthesized unsymmetrical bis(arylimino)acenaphthylene-cobalt catalysts,[2,25,27,28,33–36] the molecular weights and catalytic activities for **B** [–CH(Ph)$_2$] and **E** [–CH(*p*-FPh)$_2$] (Chart 1) are illustrated together with those corresponding to the current **I** system [–CH(*p*-MeOPh)$_2$] in Fig. 13. It should be stressed that the properties of the precatalysts were evaluated in comparable conditions with MAO as a cocatalyst. Among these precatalysts, **I** [–CH(*p*-MeOPh)$_2$] shows the highest activity, therefore it can be concluded that the introduction of the methoxy group is beneficial. In comparison, the precatalyst bearing benzhydryl group **B** [–CH(Ph)$_2$] exhibits much lower activity and the **E** [–CH(*p*-FPh)$_2$] produces polyethylene of the lowest molecular weight – see Fig. 13.

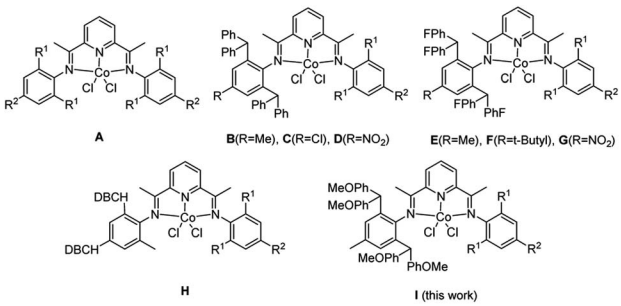

Chart 1 Development of bis(imino)pyridylcobalt(II) precatalysts, **A–I**.

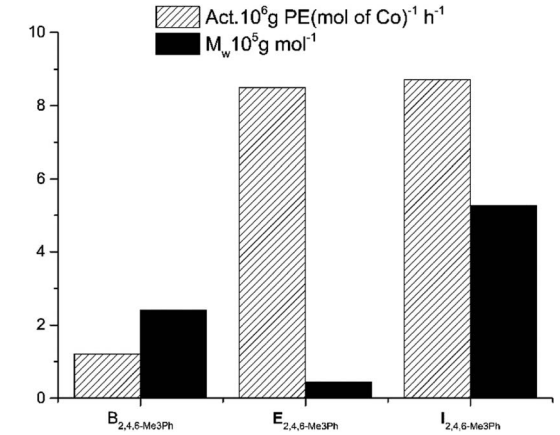

Fig. 13 Comparison of the catalytic performance of the current system with the previously reported analogues (B, E and I, see Chart 1).

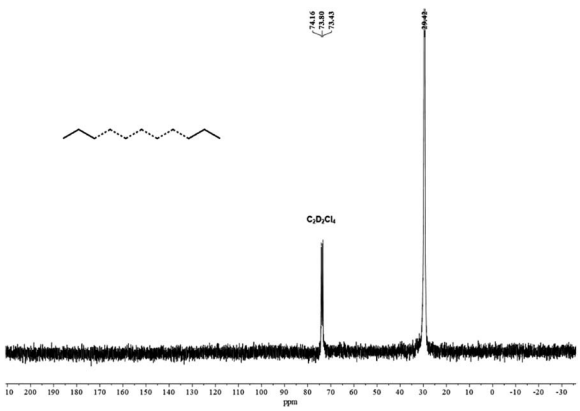

Fig. 14 ^{13}C NMR spectrum of the polyethylene produced by **Co4**/MAO (in $C_2D_2Cl_4$ at 100 °C; entry 9, Table 3).

3.2.4 Structural features of polyethylene. To analyze the branching degree of the resultant polyethylene, both DSC measurement and high-temperature ^{13}C NMR spectroscopy investigations were conducted. Examination of the polymers obtained using **Co1–Co6** with either MAO or MMAO reveals that the melting point (T_m) falls in the range from 134.6 to 136.3 °C, which suggests that the polymer is highly linear. Such result is consistent with the previous reports related to the similar cobalt precatalysts.[15,41,48] To verify our finding, the high-temperature ^{13}C NMR spectroscopy (Fig. 14) was performed on the sample obtained with the most active catalyst, namely **Co4**/MAO at 60 °C (entry 9, Table 3). The results also indicate highly linear polymer without the characteristic signal of the terminal vinyl group.

4 Conclusions

The series of cobalt-based ethylene polymerization precatalysts ligated by bis(imino)pyridine, whose one imine nitrogen atom is substituted with the 2,6-bis(4,4′-dimethoxybenzhydryl)-4-methyl phenyl group and the group attached to the other nitrogen atom is varied in terms of its steric and electronic profile, has been synthesized and characterized. On activation with MMAO or MAO, the complexes show high activity (up to 8.71×10^6 g of PE (mol of Co)$^{-1}$ h^{-1}) in the ethylene polymerization process and the resultant polyethylene exhibits the molecular weight of up to 5.27×10^5 g mol^{-1}. In comparison with the literature, the introduction of the methoxy group enhances the catalytic activity of the corresponding complexes and increases the molecular weight of polyethylene obtained. This finding provides important guidance and direction for the design and development of catalysts in the future.

Author contributions

Shi-Fang Yuan: project administration: conceptual design; writing – original draft. Luyao Wang: investigation: synthesis and characterizations of compounds. Yi Yan: investigation: characterization of polyethylene and polymeric property. Tian Liu: investigation: ethylene polymerization. Zygmunt Flisak: investigation: revised draft. Yanping Ma: investigation: ethylene polymerization and characterizations of polyethylenes. Wen-Hua Sun: project administration: conceptual design; manuscript.

Conflicts of interest

All authors declared that they have no conflict of interest.

Acknowledgements

The National Natural Science Foundation of China (No. 21871275) supported this work.

Notes and references

1 L. K. Johnson, C. M. Killian and M. Brookhart, *J. Am. Chem. Soc.*, 1995, **117**, 6414–6415.
2 B. L. Small, M. Brookhart and A. M. A. Bennett, *J. Am. Chem. Soc.*, 1998, **120**, 4049–4050.
3 G. J. P. Britovsek, V. C. Gibson, S. J. McTavish, G. A. Solan, A. J. P. White, D. J. Williams, B. S. Kimberley and P. J. Maddox, *Chem. Commun.*, 1998, 849–850.
4 V. C. Gibson, C. Redshaw and G. A. Solan, *Chem. Rev.*, 2007, **107**, 1745–1776.
5 C. Bianchini, G. Giambastiani, L. Luconi and A. Meli, *Coord. Chem. Rev.*, 2010, **254**, 431–455.
6 W. Zhang, W.-H. Sun and C. Redshaw, *Dalton Trans.*, 2013, **42**, 8988–8997.
7 J. Ma, C. Feng, S. Wang, K. Q. Zhao, W.-H. Sun, C. Redshaw and G. A. Solan, *Inorg. Chem. Front.*, 2014, **1**, 14–34.
8 Z. Flisak and W.-H. Sun, *ACS Catal.*, 2015, **5**, 4713–4724.
9 B. L. Small, *Acc. Chem. Res.*, 2015, **48**, 2599–2611.
10 F. Huang, Q. Xing, T. Liang, Z. Flisak, B. Ye, X. Hu, W. Yang and W.-H. Sun, *Dalton Trans.*, 2014, **43**, 16818–16829.
11 Z. Wang, G. A. Solan, W. Zhang and W.-H. Sun, *Coord. Chem. Rev.*, 2018, **363**, 92–108.

12 W. Zhang, W. Chai, W.-H. Sun, X. Hu, C. Redshaw and X. Hao, *Organometallics*, 2012, **31**, 5039–5048.
13 W.-H. Sun, S. Kong, W. Chai, T. Shiono, C. Redshaw, X. Hu, C. Guo and X. Hao, *Appl. Catal., A*, 2012, **447–448**, 67–73.
14 J. Ba, S. Du, E. Yue, X. Hu, Z. Flisak and W.-H. Sun, *RSC Adv.*, 2015, **5**, 32720–32729.
15 S. F. Yuan, Z. Fan, Y. Yan, Y. Ma, M. Han, T. Liang and W.-H. Sun, *RSC Adv.*, 2020, **10**, 43400–43411.
16 Y. Zhang, H. Suo, F. Huang, T. Liang, X. Hu and W.-H. Sun, *J. Polym. Sci., Part A: Polym. Chem.*, 2017, **55**, 830–842.
17 F. Huang, W. Zhang, E. Yue, T. Liang, X. Hu and W.-H. Sun, *Dalton Trans.*, 2016, **45**, 657–666.
18 F. Huang, W. Zhang, Y. Sun, X. Hu, G. A. Solan and W.-H. Sun, *New J. Chem.*, 2016, **40**, 8012–8023.
19 V. K. Appukuttan, Y. Liu, B. C. Son, C. S. Ha, H. Suh and I. Kim, *Organometallics*, 2011, **30**, 2285–2294.
20 S. Du, X. Wang, W. Zhang, Z. Flisak, Y. Sun and W.-H. Sun, *Polym. Chem.*, 2016, **7**, 4188–4197.
21 S. Du, W. Zhang, E. Yue, F. Huang, T. Liang and W.-H. Sun, *Eur. J. Inorg. Chem.*, 2016, 1748–1755.
22 Z. Wang, G. A. Solan, Q. Mahmood, Q. Liu, Y. Ma, X. Hao and W.-H. Sun, *Organometallics*, 2018, **37**, 380–389.
23 M. Khoshsefat, Y. Ma and W.-H. Sun, *Coord. Chem. Rev.*, 2021, **434**, 213788.
24 J. Yu, H. Liu, W. Zhang, X. Hao and W.-H. Sun, *Chem. Commun.*, 2011, **47**, 3257–3259.
25 J. Yu, W. Huang, L. Wang, C. Redshaw and W.-H. Sun, *Dalton Trans.*, 2011, **40**, 10209–10214.
26 X. Cao, F. He, W. Zhao, Z. Cai, X. Hao, T. Shiono, C. Redshaw and W.-H. Sun, *Polymer*, 2012, **53**, 1870–1880.
27 F. He, W. Zhao, X.-P. Cao, T. Liang, C. Redshaw and W.-H. Sun, *J. Organomet. Chem.*, 2012, **713**, 209–216.
28 Q. Mahmood, Y. P. Ma, X. Hao and W.-H. Sun, *Appl. Organomet. Chem.*, 2019, **33**, e4857.
29 W. Zhao, J. Yu, S. Song, W. Yang, H. Liu, X. Hao, C. Redshaw and W.-H. Sun, *Polymer*, 2012, **53**, 130–137.
30 J. Lai, W. Zhao, W. Yang, C. Redshaw, T. Liang, Y. Liu and W.-H. Sun, *Polym. Chem.*, 2012, **3**, 787–793.
31 S. Wang, B. Li, T. Liang, C. Redshaw, Y. Li and W.-H. Sun, *Dalton Trans.*, 2013, **42**, 9188–9197.
32 W.-H. Sun, W. Zhao, J. Yu, W. Zhang, X. Hao and C. Redshaw, *Macromol. Chem. Phys.*, 2012, **213**, 1266–1273.
33 S. Wang, W. Zhao, X. Hao, B. Li, C. Redshaw, Y. Li and W.-H. Sun, *J. Organomet. Chem.*, 2013, **731**, 78–84.
34 Q. Y. Zhang, Y. P. Ma, H. Y. Suo, G. A. Solan, T. L. Liang and W.-H. Sun, *Appl. Organomet. Chem.*, 2019, **33**, e5134.
35 R. D. Zhang, Y. P. Ma, M. Y. Han, G. A. Solan, Y. P. Ma, Y. Sun and W.-H. Sun, *Appl. Organomet. Chem.*, 2019, **33**, e5157.
36 M. Zada, L. W. Guo, Y. P. Ma, W. J. Zhang, Z. Flisak, Y. Sun and W.-H. Sun, *Molecules*, 2019, **24**, 2007.
37 W. Zhang, S. Wang, S. Du, C. Y. Guo, X. Hao and W.-H. Sun, *Macromol. Chem. Phys.*, 2014, **215**, 1797–1809.
38 W. Zhao, E. Yue, X. Wang, W. Yang, Y. Chen, X. Hao, X. Cao and W.-H. Sun, *J. Polym. Sci., Part A: Polym. Chem.*, 2017, **55**, 988–996.
39 T. E. Müller, K. C. Hultzsch, M. Yus, F. Foubelo and M. Tada, *Chem. Rev.*, 2008, **108**, 3795.
40 S. F. Yuan, Z. Fan, M. Han, Y. Yan, Z. Flisak, Y. Ma, T. Liang and W.-H. Sun, *Eur. J. Inorg. Chem.*, 2021, **16**, 1571–1580.
41 T. Liu, Y.-P. Ma, G. A. Solan, T. Liang and W.-H. Sun, *Appl. Organomet. Chem.*, 2021, **35**, e6259.
42 G. M. Sheldrick, *Acta Crystallogr., Sect. A: Found. Adv.*, 2015, **71**, 3.
43 G. M. Sheldrick, *Acta Crystallogr., Sect. C: Struct. Chem.*, 2015, **71**, 3.
44 W.-H. Sun, W. Zhao, J. Yu, W. Zhang, X. Hao and C. Redshaw, *Macromol. Chem. Phys.*, 2012, **213**, 1266–1273.
45 S. Du, S. Kong, Q. Shi, J. Mao, C. Guo, J. Yi, T. Liang and W.-H. Sun, *Organometallics*, 2015, **34**, 582–590.
46 M. Han, Q. Zhang, I. I. Oleynik, H. Suo, G. A. Solan, I. V. Oleynik, Y. Ma, T. Liang and W.-H. Sun, *Dalton Trans.*, 2020, **49**, 4774–4784.
47 H. Suo, I. I. Oleynik, C. Bariashir, I. V. Oleynik, Z. Wang, G. A. Solan, Y. Ma, T. Liang and W.-H. Sun, *Polymer*, 2018, **149**, 45–54.
48 Y. Yan, S. F. Yuan, M. Liu, G. A. Solan, Y. P. Ma, T. L. Liang and W.-H. Sun, *Chin. J. Polym. Sci.*, 2022, **40**, 266–279.
49 J. Guo, Z. Wang, W. Zhang, I. I. Oleynik, A. Vignesh, I. V. Oleynik, X. Hu, Y. Sun and W.-H. Sun, *Molecules*, 2019, **24**, 1176.
50 C. Bariashir, Z. Wang, H. Suo, M. Zada, G. A. Solan, Y. Ma, T. Liang and W.-H. Sun, *Eur. Polym. J.*, 2019, **110**, 240–251.
51 Y. Huang, R. Zhang, T. Liang, X. Hu, G. A. Solan and W.-H. Sun, *Organometallics*, 2019, **38**, 1143–1150.
52 M. Zada, A. Vignesh, H. Suo, Y. Ma, H. Liu and W.-H. Sun, *Mol. Catal.*, 2020, **492**, 110981.
53 M. Han, Q. Zhang, I. I. Oleynik, H. Suo, I. V. Oleynik, G. Solan, Y. Ma, T. Liang and W.-H. Sun, *Catalysts*, 2020, **10**, 1002.
54 S. Zhang, W.-H. Sun, T. Xiao and X. Hao, *Organometallics*, 2010, **29**, 1168–1173.
55 Q. Mahmood, E. Yue, J. Guo, W. Zhang, Y. Ma, X. Hao and W.-H. Sun, *Polymer*, 2018, **159**, 124–137.